Metabolic Engineering 47 (2018) 488–495

Contents lists available at ScienceDirect

Metabolic Engineering

journal homepage: www.elsevier.com/locate/meteng

A flow cytometric approach to engineering *Escherichia coli* for improved eukaryotic protein glycosylation

Cameron J. Glasscock[a], Laura E. Yates[a], Thapakorn Jaroentomeechai[a], Joshua D. Wilson[b], Judith H. Merritt[b], Julius B. Lucks[c], Matthew P. DeLisa[a,*]

[a] Robert F. Smith School of Chemical and Biomolecular Engineering, Cornell University, 120 Olin Hall, Ithaca, NY 14853 USA
[b] Glycobia Incorporated, 33 Thornwood Drive, Ithaca, NY 14850 USA
[c] Department of Chemical and Biological Engineering, Northwestern University, 2145 Sheridan Road, Evanston, IL 60208, USA

ARTICLE INFO

Keywords:
Asparagine-linked protein glycosylation
Glycoengineering
Glycoprotein expression
Glycosyltransferase
Oligosaccharyltransferase
Post-translational modification
Synthetic biology

ABSTRACT

A synthetic pathway for production of the eukaryotic trimannosyl chitobiose glycan (mannose$_3$-*N*-acetylglucosamine$_2$, Man$_3$GlcNAc$_2$) and its transfer to specific asparagine residues in target proteins was previously engineered in *Escherichia coli*, providing this simple microbe with the ability to perform a complex post-translational protein modification. Here, we leveraged a flow cytometric fluorescence-based assay to improve Man$_3$GlcNAc$_2$ glycan biosynthesis in *E. coli* cells. Specifically, pathway improvements were identified, including reducing pathway enzyme expression levels and overexpressing nucleotide sugar biosynthesis genes, which enhanced production of lipid-linked Man$_3$GlcNAc$_2$ by nearly 50-fold to 13.9 μg/L. In turn, cells producing higher levels of the Man$_3$GlcNAc$_2$ substrate yielded up to 10 times more glycosylated acceptor protein (to ~ 14 mg/L) than their non-optimized counterparts. These results demonstrate the use of flow cytometry screening as a powerful tool for interrogating the surfaces of glyco-engineered bacteria and identifying meaningful improvements in glycan biosynthesis. We anticipate this approach will enable further optimization of bacterial glycan biosynthesis pathways using new strain engineering tools from metabolic engineering and synthetic biology.

1. Introduction

Asparagine-linked (*N*-linked) glycosylation is a widespread post-translational modification that affects the fold and function of proteins (Helenius and Aebi, 2001; Wormald and Dwek, 1999; Xu and Ng, 2015). *N*-linked glycosylation is also important for therapeutic protein development, since many proteins must be glycosylated to function as intended (Dalziel et al., 2014). Therapeutic glycoproteins are typically produced with eukaryotic expression systems that natively possess the machinery for human-like *N*-linked glycosylation, but can be difficult to manipulate (Sethuraman and Stadheim, 2006). This difficulty is further compounded by the fact that, despite many impressive achievements (Hamilton et al., 2003; Yang et al., 2015; Meuris et al., 2014), most *N*-linked glycoprotein expression platforms produce heterologous products containing multiple glycoforms (Mimura et al., 2018; Zhang et al., 2016; Rich and Withers, 2009; Rudd and Dwek, 1997). Glycosylation is not limited to eukaryotes, however, and *N*-linked glycosylation pathways can be found in many proteobacteria (Abu-Qarn et al., 2008) and functionally transferred into *Escherichia coli* (Wacker et al., 2002). This latter development has paved the way for studying and engineering the protein glycosylation mechanism in this genetically tractable host (Feldman et al., 2005) and has potential for unlocking the use of robust prokaryotic molecular biology tools to achieve greater control over *N*-linked glycosylation (Keys and Aebi, 2017; Baker et al., 2013; Merritt et al., 2013; Terra et al., 2012).

Previous glycoengineering efforts in *E. coli* led to the development of a synthetic pathway that enables site-specific glycosylation of proteins with mannose$_3$-*N*-acetylglucosamine$_2$ (Man$_3$GlcNAc$_2$) (Valderrama-Rincon et al., 2012), a structure that comprises the core of all human *N*-linked glycans (Song et al., 2015). This heterologous pathway is comprised of multiple glycosyltransferases (GTases) from yeast and the oligosaccharyltransferase (OTase), PglB, from *Campylobacter jejuni,* an archetype for bacterial *N*-linked glycosylation. The Man$_3$GlcNAc$_2$ protein glycosylation pathway can be divided into three distinct stages: glycan biosynthesis, membrane translocation of glycans, and glycan transfer onto polypeptide acceptor sequons (Fig. 1). In the first stage, Man$_3$GlcNAc$_2$ glycans are sequentially assembled in the form of undecaprenyl-pyrophosphate (Und-PP) lipid-linked oligosaccharides (LLOs) on the cytoplasmic face of the inner membrane. This involves four heterologous GTase enzymes from *S. cerevisiae* (Alg13, Alg14, Alg1

* Corresponding author.
E-mail address: md255@cornell.edu (M.P. DeLisa).

https://doi.org/10.1016/j.ymben.2018.04.014
Received 7 February 2018; Received in revised form 17 April 2018; Accepted 19 April 2018
Available online 25 April 2018

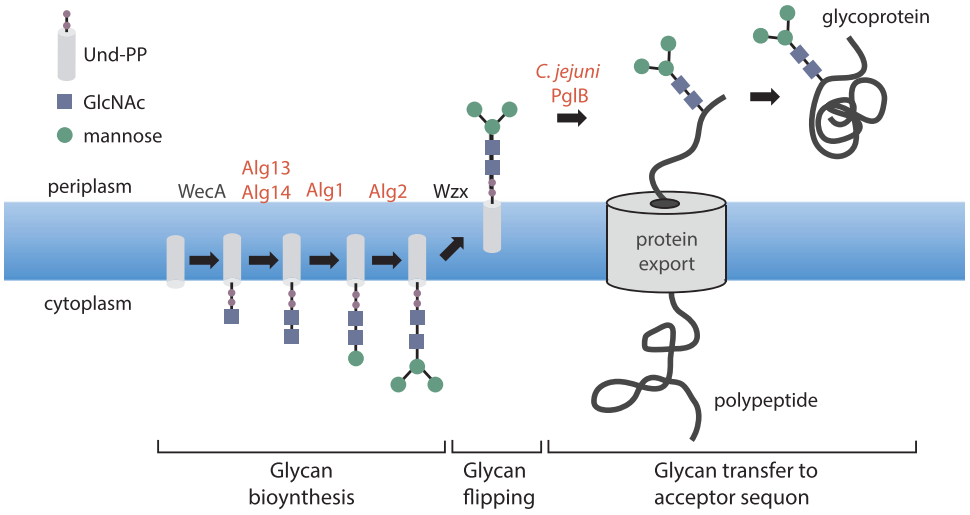

Fig. 1. The pathway for eukaryotic *N*-linked protein glycosylation in *E. coli*. The $Man_3GlcNAc_2$ protein glycosylation pathway can be divided into three distinct stages: glycan biosynthesis, membrane translocation of glycans, and glycan transfer onto polypeptide acceptor sequons. In the first stage, $Man_3GlcNAc_2$ glycans are assembled on the lipid carrier Und-PP on the cytoplasmic face of the inner membrane by yeast GTases Alg13, Alg14, Alg1, Alg2, along with endogenous *E. coli* enzyme WecA. In the second stage, lipid-linked $Man_3GlcNAc_2$ glycans are flipped to the periplasmic side of the inner membrane by the action of the flippase Wzx. In the third stage, the OTase PglB transfers $Man_3GlcNAc_2$ glycans from Und-PP to asparagine residues of acceptor proteins that are exported into the periplasm. Protein glycosylation can occur in a co- or post-translational manner, involving acceptor site sequences having a consensus of D/E-X_1-N-X_2-S/T (where X_1 and X_2 can be any amino acid but proline).

and Alg2) that catalyze the sequential addition of nucleotide-activated sugars and are encoded on the arabinose-inducible plasmid pYCG. In the subsequent glycan-flipping stage, the native *E. coli* flippase enzyme Wzx translocates newly synthesized LLOs to the periplasmic face of the inner membrane. Finally, for glycan transfer, the OTase enzyme PglB from *C. jejuni* transfers the glycan from its lipid anchor to an asparagine residue on the periplasmically expressed substrate protein.

Despite successful eukaryotic protein glycosylation, this initial report resulted in a low fraction of glycosylated protein (< 1%) and yield of 50 μg/L that was difficult to detect without extensive purification. We suspected that this inefficient glycosylation (relative to > 50% glycosylation efficiency often observed in other prokaryotic *N*-linked glycosylation systems (Mills et al., 2016, Ollis et al., 2015)) was due in part to relatively poor accumulation of the lipid-linked $Man_3GlcNAc_2$ substrate during the glycan biosynthesis stage of the engineered pathway. Here, we sought to relieve this bottleneck and improve overall protein glycosylation levels by leveraging a cell-based fluorescence assay to screen for improvements made possible through manipulating enzyme expression and host metabolism. Specifically, we reduced the expression levels of the four heterologous yeast GTases and overexpressed two endogenous biosynthetic enzymes for GDP-mannose precursor synthesis. The combined effect of these changes was a 4-fold increase in cell surface $Man_3GlcNAc_2$ levels that was found to correlate with a nearly 50-fold increase in intracellular UndPP-linked $Man_3GlcNAc_2$. In cells producing higher levels of the $Man_3GlcNAc_2$ substrate, protein glycosylation was also significantly enhanced with yields of glycosylated acceptor protein that were more than 8–10 times greater than the yields achieved in non-optimized cells. Overall, we expect that our results will provide a robust engineering framework for future efforts to develop efficient eukaryotic protein glycosylation pathways in *E. coli* cells.

2. Material and methods

2.1. Bacterial strains and growth conditions

E. coli strains MC4100 *gmd::kan* and MC4100 *gmd::kan ΔwaaL* (Valderrama-Rincon et al., 2012) as well as strains Origami2(DE3) *gmd::kan* and Origami2(DE3) *gmd::kan ΔwaaL* (Hamilton et al., 2017) were all developed previously and used here. Chemically competent versions of these *E. coli* strains were transformed with plasmid combinations, plated on Luria-Bertani (LB)-agar (BD Difco) containing 100 μg/mL carbenicillin, and/or 34 μg/mL chloramphenicol. Following overnight incubation at 37 °C, plates were taken out of the incubator and left at room temperature for approximately 8 h. Three colonies were picked and used to inoculate 500 μL of LB containing appropriate antibiotics at the concentrations above in a 2-mL 96-well block (Costar), and grown approximately 17 h overnight at 37 °C and 1000 rpm in a Vortemp 56 benchtop shaker (Labnet International). Ten μL of each overnight culture was then added to separate wells on a new block containing 490 μL (1:50 dilution) of LB containing antibiotics and grown for 18 h at 30 °C and 1000 rpm in a Vortemp 56 benchtop shaker (Labnet International). Cells containing plasmid pYCG were induced by the addition of 0.2% L-arabinose at inoculation. 200 μL of each sample was spun down and washed once with 200 μL PBS buffer before resuspension in 200 μL PBS. Ten μL of each well were then transferred into 96-well plates (Costar) with 90 μL of PBS containing 3 μg/mL AlexaFluor-488 conjugated concanavalin A (ConA) lectin (Sigma) and incubated at 37 °C and 1000 rpm for 30 min in a Vortemp 56 benchtop shaker (Labnet International). Absorbance at 600 nm (Abs_{600}) was measured for each well on a plate reader (BioTek Synergy).

2.2. Plasmid construction

Plasmid pYCG is described elsewhere (Valderrama-Rincon et al., 2012). Plasmids pConYCG and pConYCGmCB were constructed using Gibson assembly in a manner analogous to the construction of pYCG (Valderrama-Rincon et al., 2012). All important DNA sequences in these plasmids are listed in Supplementary Table 1. The constitutive promoter sequences were from the Anderson promoter library from the Registry of Standard Biological Parts (partsregistry.org) (Kelly et al., 2009). The genes encoding ManB and ManC were PCR amplified from the *E. coli* MG1655 *cps* operon. Plasmid pMAF10, which encodes *C. jejuni* PglB, is described elsewhere (Feldman et al., 2005). Plasmid pTrc-spDsbA-MBP-GCG^{DQNAT} was generated using standard homologous recombination in *S. cerevisiae* as previously described (Shanks et al., 2006). Briefly, DNA encoding the DsbA signal peptide and *E. coli* maltose-binding protein (MBP; encoded by the *malE* gene) were amplified with primers containing homology to vector pTrc99Y (Valderrama-Rincon et al., 2012). Similarly, human glucagon (GCG; residues 1–29) was amplified from a synthetic oligonucleotide with primers that introduced DNA encoding a C-terminal DQNAT glycosylation tag (GlycTag) (Fisher et al., 2011) and 6 × -His tag followed by DNA with homology to pTrc99Y. These PCR products were used with linearized pTrc99Y to co-transform *S. cerevisiae* for cloning by homologous recombination to generate plasmid pTrc-spDsbA-MBP-GCG^{DQNAT}.

2.3. Flow cytometric analysis and microscopy

Five μL from each 96-well plate was diluted into 195 μL PBS in a new FACS round-bottom 96-well plate. The plate was read on an Accuri C6 Plus flow cytometer (BD Biosciences). Data for the following parameters were collected on the flow cytometer: forward scatter (FSC), side scatter (SSC), and AlexaFluor-488 fluorescence (488 nm excitation, 525 nm emission). Three to ten μL of each sample was measured. All samples were collected with 10,000–50,000 counts. Counts were gated in FSC versus SSC by choosing a window surrounding the largest cluster of cells. Fluorescence values were recorded in relative channel number (1–262,144 corresponding to 18-bit data) and the geometric mean over the gated data was calculated for each sample. Data analysis and FACS calibration was performed as described previously (Lucks et al., 2011). Rainbow calibration particles (Spherotech) were used to obtain a calibration curve to convert fluorescence intensity (geometric mean, relative channel number) into molecules of equivalent fluorescein (MEFL) units. Mean MEFL values were calculated over replicates. All flow cytometry experiments involved three biological replicates. Extraction of Flow Cytometry Standard (FCS) files, traditional gating, analysis of calibration beads data, standard curve generation, transformation to MEFL, and generation of histograms was performed using FlowCal software (Castillo-Hair et al., 2016). For fluorescence microscopy, ConA-AlexaFluor labeled cells were pelleted, washed, and resuspended in 100 μL PBS buffer. Agarose pads were prepared by adding 2% low-melt agarose to culture medium and heating until melted. Thirty μL of agarose solution were then added onto a depression slide and covered with another flat slide (Fisher Scientific). Following pad solidification (~ 10 min), 5 μL of cells treated with ConA-AlexaFluor were added to the pad, and covered with a cover slip. Slides were viewed on an inverted fluorescent Leica DM-IL LED microscope with a Leica HCX PL APO 100 × /1.40 PH CS oil-immersion objective lens and high-resolution cooled Q-imaging CCD.

2.4. Isolation and analysis of LLOs

The methods for extraction of LLOs and release of the glycan from the lipid were followed as described elsewhere (Gao, 2005; Gao and Lehrman, 2006). Briefly, dried *E. coli* cell pellets from 250 mL culture were resuspended in 2:1 chloroform: methanol, sonicated, and the remaining solids collected by centrifugation. This pellet was sonicated in water and collected by centrifugation. The resulting pellet was sonicated in 10:10:3 chloroform: methanol:water to isolate the LLOs from the inner membrane. The LLOs were purified using acetate-converted DEAE anion exchange chromatography as they bind to the anion exchange resin via the phosphates that link the lipid and glycan. The resulting compound was dried and treated by mild acid hydrolysis to release glycans from the lipids (Gao, 2005; Gao and Lehrman, 2006). The released glycans were then separated from the lipid by a 1:1 butanol: water extraction, wherein the water layer contains the glycans. The glycans were then further purified with a graphitized carbon column using a 0–50% water: acetonitrile gradient. Isolated $Man_3GlcNAc_2$ glycans were analyzed by fluorophore-assisted carbohydrate electrophoresis (FACE) as described (Gao, 2005). Briefly, 20 μL of purified glycan was dried and resuspended in equal volumes of $NaCNBH_3$ and 7-amino-1,3-naphthalenedisulfonic acid (ANDS) solution. The reaction was incubated for 18 h at 37 °C, dried, and resuspended in thorin I loading dye. Gels were prepared according to the published protocol (Gao, 2005) and run at 4 °C with a constant current of 10 mAmp. Gels were visualized using a Bio-Rad ChemiDoc MP. Isolated $Man_3GlcNAc_2$ glycans were also analyzed by matrix-assisted laser desorption/ionization mass spectrometry (MALDI-MS) was performed as described (Valderrama-Rincon et al., 2012). Briefly, after desalting with Dowex 50WX8 hydrogen form, 200–400 mesh (Sigma) and AG1-X8 formate form, 200–400 mesh (Bio-Rad) resins, glycans were concentrated and MALDI-MS profiles were acquired using 2,5-dihydroxybenzoic acid (Alfa Aesar) as matrix on a 5800 MALDI-TOF/TOF (SciEx) in positive ion reflectron mode (500–3000 Da mass range). MS traces were generated and analyzed using mMass (Strohalm et al., 2008).

2.5. Glycoprotein expression and isolation

Cells carrying one of the glycan biosynthesis plasmids along with pMAF10 and pTrc-spDsbA-MBP-GCG^{DQNAT} were grown in 100 mL of LB at 37 °C until Abs_{600} reached ≈ 1.5. Culture temperature was reduced to 30 °C (and L-arabinose was added to a final concentration of 0.2% (w/v) to induce *ALG* gene expression in pYCG) and allowed to grow overnight at 30 °C. The next day, cells were induced with 0.1 mM isopropyl β-D-1-thiogalactopyranoside (IPTG) to initiate synthesis of the MBP-GCG^{DQNAT} acceptor protein. Protein expression proceeded for 8 h at 30 °C. Cells were then harvested and subjected to subcellular fractionation, which was performed as described elsewhere (Karlsson et al., 2012). Briefly, we pelleted and washed 100 mL of IPTG-induced culture with subcellular fractionation buffer (0.2 M Tris-Ac (pH 8.2), 0.25 mM EDTA, and 0.25 M sucrose, and 160 μg/mL lysozyme). Cells were resuspended in 1.5 mL subcellular fractionation buffer and then incubated for 5 min on ice and spun down. After addition of 60 μL of 1 M $MgSO_4$, cells were incubated for 10 min on ice. Cells were spun down, and the supernatant was taken as the periplasmic fraction. To isolate glycoproteins, periplasmic fractions were subjected to affinity chromatography with a Qiagen Ni-NTA kit. Eluates were collected, solubilized in Laemmli sample buffer containing 5% β-mercaptoethanol, and resolved on SDS-polyacrylamide gels.

2.6. Western blot analysis

Purified protein samples were separated using 8% SDS-PAGE gels and transferred to PVDF membranes. Proteins that harbored 6 × -His affinity tags were detected with a monoclonal anti-polyhistidine-horse radish peroxidase (HRP) conjugate (Abcam) per manufacturers' instructions. Protein-conjugated glycans were detected with 5 μg/mL ConA-HRP conjugate (Sigma).

3. Results

3.1. Cell-surface glycan display for screening $Man_3GlcNAc_2$ levels in living cells

To probe the abundance of $Man_3GlcNAc_2$ LLOs produced in living cells, we employed a flow cytometric assay for cell-surface display of $Man_3GlcNAc_2$ glycans (Valderrama-Rincon et al., 2012) (Fig. 2**a**). This assay takes advantage of the fact that Gram-negative bacterial cell surfaces can have engineered oligosaccharides in their lipopolysaccharide (LPS) layer (Fisher et al., 2011; Ilg et al., 2010). Such remodeled LPS depends on the O-antigen ligase WaaL, which transfers periplasmic Und-PP-linked oligosaccharides onto lipid A. These oligosaccharides are shuttled to the cell surface via the LPS transport system, after which they can be conveniently labeled and detected by flow cytometry (Fisher et al., 2011; Ilg et al., 2010).

Consistent with previous observations (Valderrama-Rincon et al., 2012), MC4100 *gmd::kan* cells carrying pYCG but not control cells carrying an empty vector were fluorescent upon labeling with fluorophore-conjugated ConA (Fig. 2**b**), which preferentially binds internal and non-reducing terminal α-mannose in oligosaccharides. Fluorescence microscopy revealed that ConA binding was clearly localized on the cell surface (Supplementary Fig. 1). During these studies, we also noticed that MC4100 *gmd::kan* cells expressing pYCG exhibited variable mean fluorescence intensities across biological replicates and a bimodal fluorescence distribution (Fig. 2**b** and Supplementary Fig. 2a), indicating genetic instability in the pYCG construct, as well as poor growth following arabinose induction (Supplementary Fig. 3). In

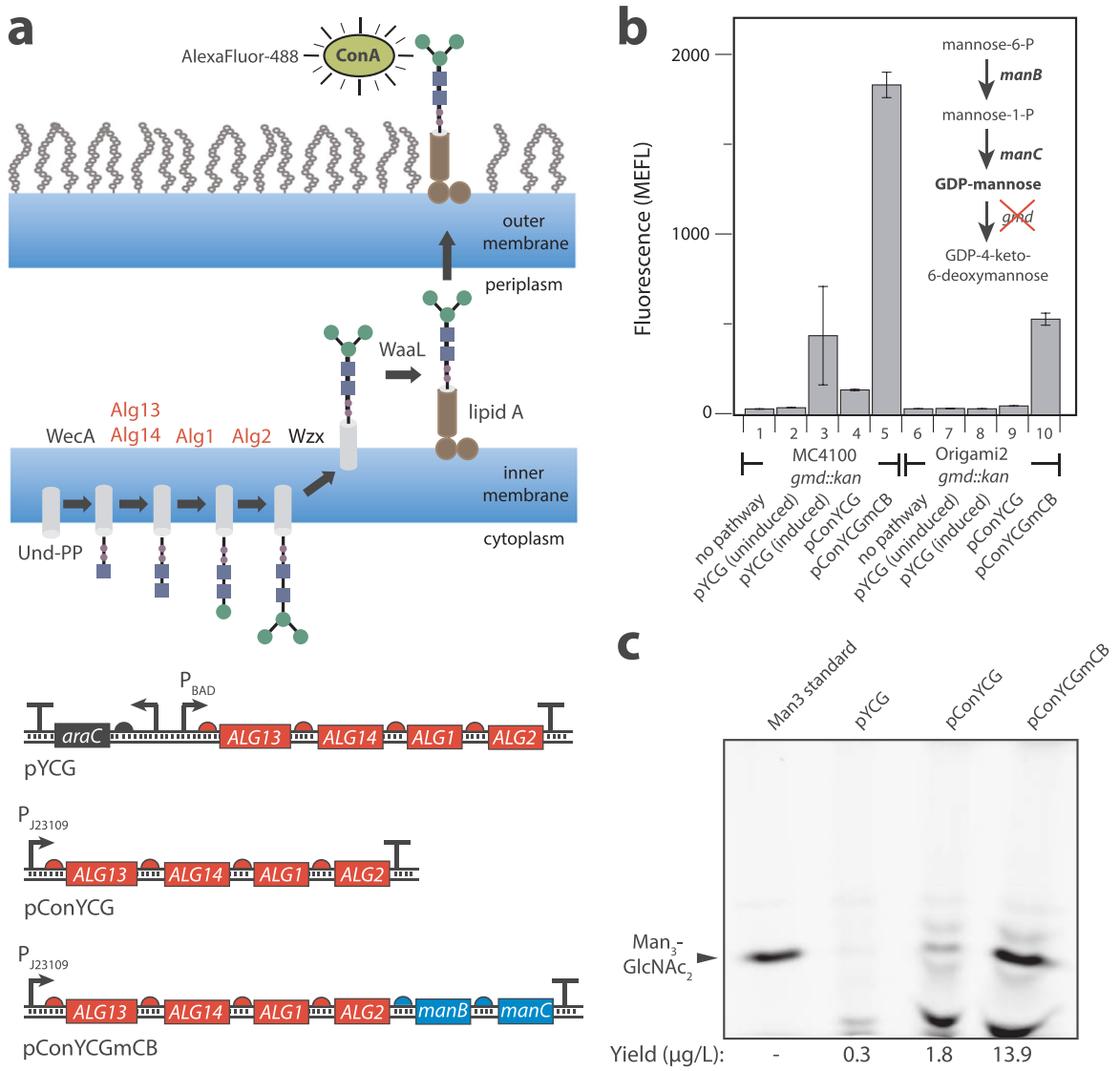

Fig. 2. Screening of $Man_3GlcNAc_2$ pathway variants with glycan display. (a) (upper panel) Scheme for flow cytometric analysis of glycan cell-surface display. Cytoplasmic LLOs are a substrate for Wzx-mediated translocation across the inner membrane into the periplasm. Glycans are subsequently transferred to lipid A by the endogenous O-antigen ligase WaaL and shuttled to the cell surface where they become available for labeling with AlexaFluor-488 conjugated ConA. ConA labeled cells are readily analyzed by flow cytometry. (lower panel) Plasmid architecture for pYCG, pConYCG, and pConYCGmCB. For pYCG, expression of the artificial *ALG13-ALG14-ALG1-ALG2* operon is driven by an arabinose-inducible P_{BAD} promoter. For pConYCG, the P_{BAD} promoter and *araC* repressor gene in pYCG are replaced by a low-strength constitutive promoter J23109 from the Registry of Standard Biological Parts (partsregistry.org). For pConYCGmCB, genes encoding *manB* and *manC* were PCR amplified from *E. coli* MG1655 and cloned into pConYCG, just after the *ALG13-ALG14-ALG1-ALG2* pathway operon. (b) Mean molecules of equivalent fluorescein (MEFL) for MC4100 *gmd::kan* or Origami2 *gmd::kan* cells containing: no pathway control (strains 1,6); pYCG uninduced (strains 2,7); pYCG induced (strains 3,8); pConYCG (strains 4,9); or pConYCGmCB (strains 5,10). All strains were grown in LB and labeled with ConA before flow cytometric analysis. Strains carrying pYCG were induced at inoculation with 0.2% L-arabinose. Error bars represent standard error of at least three biological replicates. Inset pathway details GDP-mannose biosynthesis by phosphoglucoisomerase (PGI), mannose-6-phosphate isomerase (ManA), phosphomannomutase (ManB), and mannose-1-phosphate guanylyltransferase (ManC). A knockout of GDP-mannose 4,6-dehydratase (GMD) prevents conversion of GDP-mannose into GDP-4-keto-6-deoxymannose. (c) FACE gel analysis of $Man_3GlcNAc_2$ glycans produced by MC4100 *gmd::kan* Δ*waaL* cells carrying pYCG, pConYCG, or pConYCGmCB as indicated. Glycans were isolated by extraction of LLOs from each strain followed by acid hydrolysis to release the glycan moiety. An equivalent volume was added to each lane. A total of 0.5 µg of commercial $Man_3GlcNAc_2$ was used as a standard for quantification. Yields of each glycan were estimated by densitometry analysis of individual bands using Image Lab 6.0.

addition, we noticed that cells carrying pYCG underwent a change in cell morphology (Supplementary Fig. 2b), as evidenced by a comparison of forward scatter (FSC) and side scatter (SSC) profiles with cells containing an empty vector, which was indicative of cellular stress.

We speculated that this observed instability was due to high-level expression from the arabinose-inducible P_{BAD} promoter in pYCG that drives expression of the four *S. cerevisiae* GTases (Fig. 2**a**). To remedy this issue, we replaced the P_{BAD} promoter in pYCG with the low-strength constitutive promoter pJ23109 from the Anderson promoter library from the Registry of Standard Biological Parts (partsregistry.org) (Kelly et al., 2009), yielding a new plasmid for $Man_3GlcNAc_2$ biosynthesis called pConYCG (Fig. 2**a**). It should be noted that we were unable to clone stronger constitutive promoters from the Registry of Standard Biological Parts without the accumulation of mutations in the pathway. Flow cytometric analysis of cells carrying pConYCG exhibited a lower mean fluorescence intensity compared to cells carrying pYCG; however, these cells displayed a more stable fluorescence phenotype as evidenced by reduced error between samples and a uniform

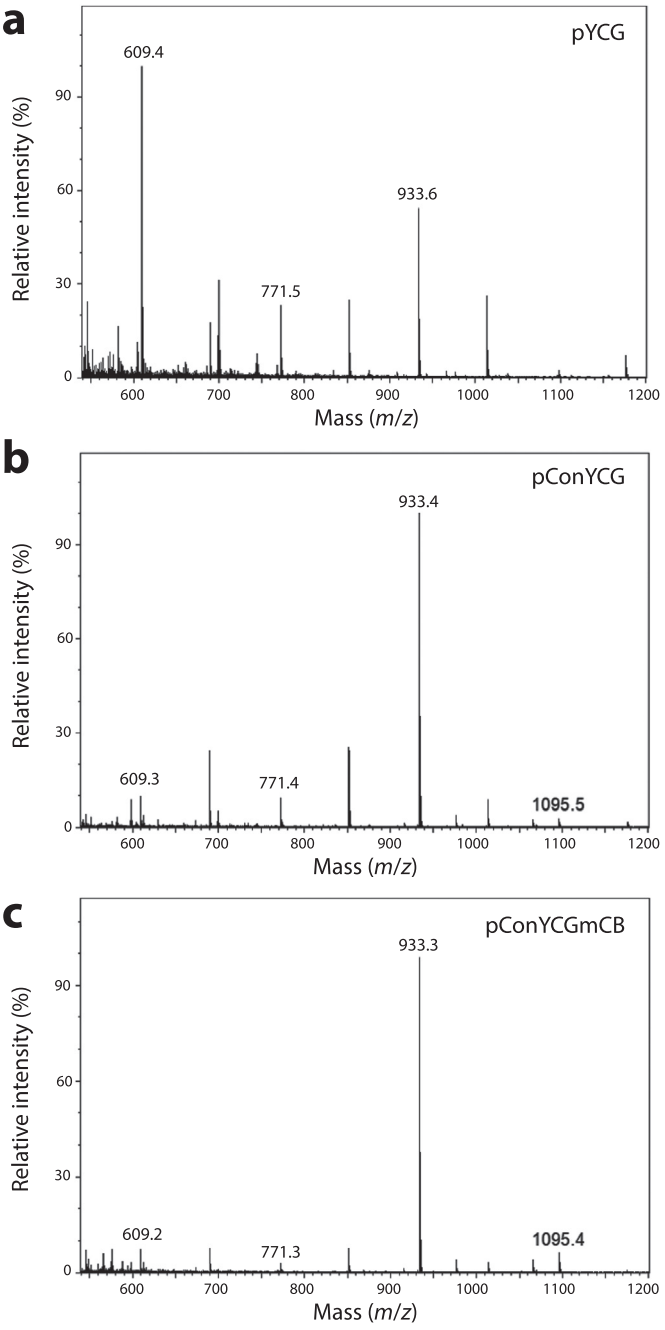

Fig. 3. MS analysis of glycans isolated from glycoengineered *E. coli* strains. MALDI-MS profiles of *N*-glycans derived from *E. coli* MC4100 *gmd::kan* Δ*waaL* cells carrying (a) pYCG, (b) pConYCG, or (c) pConYCGmCB as indicated. Glycans were obtained by first extracting LLOs from each of the different strains followed by separating the glycans from the lipid carrier by mild acid hydrolysis. The signals at *m/z* of 609, 771, 933, and 1095 correspond to $Hex_1HexNAc_2$, $Hex_2HexNAc_2$, $Hex_3HexNAc_2$, and $Hex_4HexNAc_2$, respectively.

fluorescence distribution (Fig. 2**b** and Supplementary Fig. 2a). In addition, cells expressing pConYCG showed virtually no change in cell morphology by FSC/SSC profile (Supplementary Fig. 2b) and achieved much higher cell densities than their pYCG counterparts (Supplementary Fig. 3). Based on the improvements in growth and phenotypic stability, we chose to proceed with pConYCG.

3.2. Increasing $Man_3GlcNAc_2$ LLO levels by ManBC overexpression

Previously, sufficient availability of the Alg1/2 substrate precursor nucleotide-activated sugar guanosine diphosphate-mannose (GDP-mannose) was ensured by knockout of the chromosomal copy of GDP-mannose-4,6-dehydratase (GMD). GMD normally shunts GDP-mannose to GDP-4-keto-6-deoxymannose in the first step of GDP-L fucose synthesis (Fig. 2**b**). In cells lacking GMD (e.g., MC4100 *gmd::kan*), levels of GDP-mannose are sufficiently elevated for producing detectable levels of $Man_3GlcNAc_2$-containing LLOs (Valderrama-Rincon et al., 2012). However, while detectable, these cells produced overall low levels of $Man_3GlcNAc_2$ (~ 0.3 mg/L) and accumulated incompletely synthesized glycans in the form of $ManGlcNAc_2$ and $Man_2GlcNAc_2$ intermediates (Valderrama-Rincon et al., 2012). We hypothesized here that these deficiencies were caused by suboptimal GDP-mannose levels resulting from low expression of the GDP-mannose biosynthetic enzymes phosphomannomutase (ManB) and mannose-1-phosphate guanylyltransferase (ManC). The low expression would be expected since the *manB* and *manC* genes are naturally encoded on the heavily-regulated *cps* operon for capsular polysaccharide synthesis and may not be very highly expressed under the conditions used in our study (Gottesman et al., 1985).

To alleviate this potential bottleneck, the operon from *E. coli* MG1655 encoding the *manB* and *manC* genes was cloned into the pConYCG pathway to create plasmid pConYCGmCB (Fig. 2**a**). MC4100 *gmd::kan* cells transformed with this plasmid were subjected to ConA labeling and flow cytometric screening. In line with our hypothesis, MC4100 *gmd::kan* cells carrying pConYCGmCB exhibited very strong cell fluorescence, which was ~ 14 times greater than the fluorescence detected for MC4100 *gmd::kan* cells carrying pConYCG (Fig. 2**b**). In addition, we noticed that cells exhibited: (i) a uniform fluorescence distribution that was localized on the cell surface (Supplementary Figs. 1 and 2a); (ii) a FSC/SSC profile that was nearly identical to negative control cells (Supplementary Fig. 2b); and (iii) robust growth (Supplementary Fig. 3). To investigate the influence of strain background on glycan biosynthesis with pYCG plasmid derivatives, we also considered the strain Origami2 *gmd::kan*, which has been used as a source of eukaryotic $Man_3GlcNAc_2$-containing LLOs for further in vitro editing (Hamilton et al., 2017). Interestingly, flow cytometric analysis of Origami2 *gmd::kan* cells carrying pYCG or pConYCG resulted in no detectable fluorescence above background (Fig. 2**b**). However, Origami2 *gmd::kan* cells carrying pConYCGmCB generated a strong fluorescence signal that was comparable to that of MC4100 *gmd::kan* cells with the same plasmid (Fig. 2**b**).

To verify that the increase in cell-surface fluorescence corresponded to greater intracellular $Man_3GlcNAc_2$ accumulation, LLOs were extracted from MC4100 *gmd::kan* Δ*waaL* cells and analyzed by FACE analysis (Gao, 2005; Gao and Lehrman, 2006). The *waaL* gene encodes an O-antigen ligase that catalyzes the transfer of Und-PP-linked oligosaccharides to lipid A; hence, deletion of this gene is expected to prevent Und-PP-linked $Man_3GlcNAc_2$ from shuttling to the outer membrane, as was shown previously (Valderrama-Rincon et al., 2012). In line with the ConA labeling experiments, the levels of lipid-linked $Man_3GlcNAc_2$ produced by MC4100 *gmd::kan* Δ*waaL* cells carrying pConYCGmCB were ~ 8- and 46-fold greater than those in MC4100 *gmd::kan* Δ*waaL* cells carrying pConYCG and pYCG, respectively, as estimated by densitometry analysis of individual bands in the FACE gel (Fig. 2**c**). Interestingly, LLO levels produced in cells containing pConYCG were ~ 6-fold higher than cells containing pYCG, in contradiction with flow cytometry results. This discrepancy may be explained by the substantial difference in cell fitness between the two strains and the variability of pYCG fluorescence observed by flow cytometry (Supplementary Fig. 3).

To verify the glycan structure produced by these strains, LLOs were extracted and characterized by MALDI-MS analysis. Consistent with previous MALDI-MS spectra (Valderrama-Rincon et al., 2012), MC4100 *gmd::kan* Δ*waaL* cells carrying pYCG produced $Hex_3HexNAc_2$, consistent with the expected $Man_3GlcNAc_2$ glycan, but also accumulated significant amounts of incompletely synthesized glycans in the form of

$Hex_1HexNAc_2$ and $Hex_2HexNAc_2$ (Fig. 3**a**). In line with the improved glycan levels, MC4100 *gmd::kan* Δ*waaL* cells carrying pConYCG or pConYCGmCB produced $Hex_3HexNAc_2$ as the primary oligosaccharide with only background levels of $Hex_1HexNAc_2$ and $Hex_2HexNAc_2$ glycoforms (Fig. 3**b** and **c**). Hence, pathway expression from the pConYCG or pConYCGmCB plasmids yielded significant levels of $Man_3GlcNAc_2$ glycan at the expense of the undesired intermediate products. Moreover, these findings confirm that the fluorescence screening identified *bona fide* improvements in $Man_3GlcNAc_2$ glycan biosynthesis and reveal the potential of flow cytometry for optimizing the first stage of *N*-linked glycosylation in bacteria.

3.3. Higher $Man_3GlcNAc_2$ levels correlate with increased protein glycosylation

To determine whether transfer of $Man_3GlcNAc_2$ glycans to secretory glycoproteins in vivo was also improved, we focused our attention on PglB from *C. jejuni* (*Cj*PglB) because it was previously reported to recognize Und-PP-linked $Man_3GlcNAc_2$ as substrate (Valderrama-Rincon et al., 2012). For the glycoprotein target, we made use of a model fusion protein comprised of *E. coli* MBP and human GCG (residues 1–29) that was modified with an N-terminal co-translational export signal from *E. coli* DsbA and a C-terminal GlycTag having the sequence DQNAT (Fisher et al., 2011). When this engineered acceptor protein was expressed in MC4100 *gmd*::kan Δ*waaL* or Origami2 *gmd*::kan Δ*waaL* cells carrying pYCG and pMAF10 encoding *Cj*PglB, glycosylation was clearly achieved as evidenced by the mobility shift of the fusion protein from the unmodified (g0) to the monoglycosylated (g1) form (Fig. 4) in Western blots probed with anti-polyhistidine (anti-His) antibody. These results were corroborated by detection of the fusion proteins with ConA (Fig. 4), which confirmed attachment of mannose-terminal glycans. Importantly, when similar experiments were performed with strains carrying the pConYCG or pConYCGmCB plasmids, we detected highly efficient glycosylation (~ 100% as determined by densitometry analysis) with no visible bands corresponding to the g0 form of the acceptor protein (Fig. 4). In addition, striking improvements in the amount of monoglycosylated product were observed for both MC4100 *gmd*::kan Δ*waaL* and Origami2 *gmd*::kan Δ*waaL* carrying pConYCGmCB (Fig. 4). The yield of glycosylated fusion protein produced by these latter strains was determined to be 14.1 and 8.0 mg/L of cell culture, respectively, which is competitive with other engineered *N*-linked glycosylation pathways in *E. coli*, such as one that produced 25 mg/L of *N*-glycosylated vaccine carrier protein bearing bacterial polysaccharides (Ihssen et al., 2010). Our values represent yield enhancements of ~ 8- and ~ 10-fold, respectively, compared to the corresponding strains carrying the pYCG plasmid. Taken together, these results confirm that the improvements in $Man_3GlcNAc_2$ biosynthesis directly translated to significantly greater accumulation of glycosylated acceptor proteins that rival yields of *E. coli*-based glycoprotein production involving bacterial polysaccharides.

4. Discussion

The engineering of *N*-linked glycosylation in bacteria holds great promise for the cost-effective biomanufacturing of conjugate vaccines and therapeutic glycoproteins (Baker et al., 2013; Merritt et al., 2013; Terra et al., 2012). However, in the seminal report describing *N*-linked glycosylation of acceptor proteins with the eukaryotic $Man_3GlcNAc_2$ glycan in *E. coli*, the yield of glycosylated proteins was reported to be ~ 50 μg/L, which amounted to only a small fraction (< 1%) of each expressed protein under the conditions tested (Valderrama-Rincon et al., 2012). It was proposed that increasing these levels would likely require, among other things, strategies for relieving enzymatic and metabolic bottlenecks and/or optimizing the glycosylation enzymes. Indeed, we showed here that overexpressing enzymes involved in GDP-mannose biosynthesis and decreasing the expression of the yeast Alg enzymes resulted in enhanced production of lipid-linked $Man_3GlcNAc_2$. In turn, the yield of glycosylated acceptor proteins produced by these optimized strains appeared to be very efficient, with ~ 100% of the acceptor protein undergoing conversion to the glycosylated form. Moreover, yields of ~ 14 mg/L were achieved in the best cases, representing a two-orders-of-magnitude improvement compared to our earlier report and rivaling the yield (25 mg/L) reported for *E. coli*-based production of carrier proteins glycosylated with bacterial polysaccharides (Ihssen et al., 2010).

To improve the glycan biosynthesis stage, we leveraged a flow cytometric assay for cell-surface displayed glycans. Historically, interrogation of this step has relied on a limited repertoire of low-

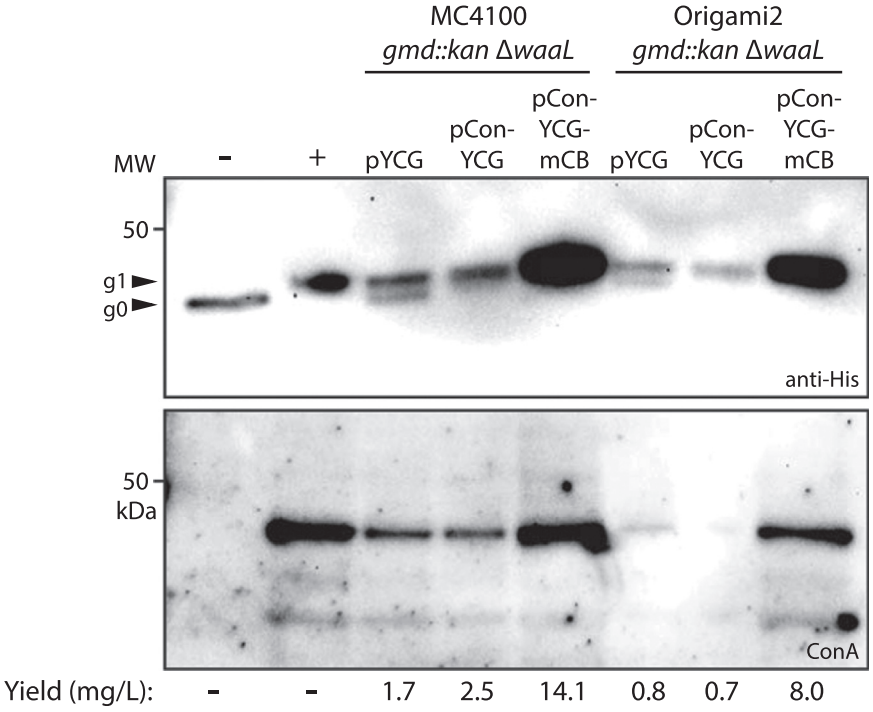

Fig. 4. Efficient glycosylation of acceptor protein with $Man_3GlcNAc_2$. Western blot analysis of MBP-GCG^{DQNAT} in periplasmic fractions isolated from *E. coli* MC4100 *gmd*::kan Δ*waaL* or Origami2 *gmd::kan* Δ*waaL* cells carrying pYCG, pConYCG, or pConYCGmCB as indicated. An equivalent volume was added to each lane. Polyhistidine tags on the proteins were detected using anti-His antibodies while mannose glycans on the proteins were detected using ConA. Molecular weight (MW) markers are indicated on left side of each blot. The expected MW for MBP-GCG^{DQNAT} is 48.5 kDa without the glycan and 49.4 kDa with $Man_3GlcNAc_2$ attached. Blots are representative of results obtained for biological triplicates. A total of 2.0 μg of purified aglycosylated or glycosylated MBP-GCG^{DQNAT} protein was added to lanes 1 and 2, respectively, and glycosylated MBP-GCG^{DQNAT} was used as a standard for quantification. Yields of each glycoprotein were estimated by densitometry analysis of individual bands using Image Lab 6.0.

throughput methods, such as Western blotting, FACE, and MS analysis, which are time consuming and labor intensive. In contrast, the use of flow cytometry for optimizing glycan biosynthesis (which can be performed over 3 days from transformation to flow cytometry with a total bench time < 5 h) adds a complementary tool that should streamline the pace at which pathways for *N*-linked glycosylation in *E. coli* can be studied and engineered. It is also worth pointing out that our approach is entirely compatible with new tools from metabolic engineering and synthetic biology for optimizing enzymes, pathways, and strains, or creating entirely new ones from scratch. This is significant because techniques for bacterial strain engineering such as multiplex automated genome engineering (MAGE) (Wang et al., 2009) or sRNA-based metabolic engineering (Na et al., 2013) often require high-throughput screens or selections to be effectively utilized. Although a potentially powerful approach, one concern with coupling high-throughput strain engineering techniques with our cell-surface display assay is the possibility of selecting for strains that are highly fluorescent, but exhibit growth impairment, as is the case for MC4100 *gmd::kan* cells containing pYCG. This issue could potentially be remedied by coupling flow cytometry screening with a simple screen/selection for bacterial fitness.

It is interesting to note that while the levels of $Man_3GlcNAc_2$ were increased by nearly 50 fold, the yield of glycosylated acceptor protein produced in these optimized host strains only increased by 8–10 fold. This discrepancy suggests the existence of additional bottlenecks after glycan biosynthesis, such as glycan flipping and glycan transfer to protein targets, that impact overall system efficiency. Fortuitously, in addition to the use of flow cytometry for engineering the first stages of *N*-linked glycosylation, several new tools have become available for engineering the later stages of protein glycosylation. These include a high-throughput assay called glycoSNAP (glycosylation of secreted *N*-linked acceptor proteins) that was used with great success to engineer *Cj*PglB variants with relaxed acceptor site specificity (Ollis et al., 2014), as well as glycophage display systems that have been used to screen acceptor-site libraries for optimal sequons (Celik et al., 2010; Durr et al., 2010). We anticipate in the future that the flow cytometric approach described here could be combined with these and/or other engineering tools to systematically uncover further improvements in our eukaryotic protein glycosylation pathway.

Here, we found that overexpression of enzymes involved in GDP-mannose biosynthesis improved the production of lipid-linked $Man_3GlcNAc_2$. We also found that tuning the expression of the Alg GTases from yeast increased biosynthesis of the $Man_3GlcNAc_2$ glycan. Further manipulation of *E. coli* metabolism by genetic techniques is likely to result in additional improvements and may become necessary for the conversion of $Man_3GlcNAc_2$ to more complex human glycan structures (i.e., by addition or substitution of heterologous GTase enzymes). We expect that the glycan biosynthesis within these elaborated pathways could be rapidly optimized in a similar fashion using flow cytometry in combination with fluorophore-conjugated lectins or antibodies with different glycan specificity. It could also be used to more efficiently guide bioprocess optimization, which has so far been limited to one-at-a-time manipulations that must be manually characterized by low-throughput methods for product detection (Ihssen et al., 2010; Kampf et al., 2015). Based on these possibilities, the future looks bright for the development of cost-effective and modular *E. coli*-based platforms for efficient biosynthesis of important glycomolecules.

Acknowledgements

The authors would like to thank members of the Lucks and DeLisa labs for helpful discussions during the process of preparing this manuscript as well as Prof. Josh Leonard and Taylor Dolberg for assistance with fluorescence microscopy. This research was supported by National Science Foundation Awards CBET-1605242 (to M.P.D.), CBET-1159581 (to M.P.D.), CBET-1402843 (to J.B.L. and M.P.D.), a National Science Foundation Graduate Research Fellowship DGE-1144153 (to C.J.G.), and a Royal Thai Government Fellowship (to T.J.).

Competing financial interests

M.P.D. has a financial interest in Glycobia, Incorporated and Versatope, Incorporated. M.P.D.'s interests are reviewed and managed by Cornell University in accordance with their conflict of interest policies.

Author contributions

C.J.G. designed research, performed research, analyzed data, and wrote the paper. T.J., L.E.Y., J.D.W. and J.H.M. designed research, performed research, and analyzed data. J.B.L. and M.P.D. designed research, analyzed data, and wrote the paper.

Appendix A. Supporting information

Supplementary data associated with this article can be found in the online version at http://dx.doi.org/10.1016/j.ymben.2018.04.014.

References

Abu-Qarn, M., Eichler, J., Sharon, N., 2008. Not just for Eukarya anymore: protein glycosylation in Bacteria and Archaea. Curr. Opin. Struct. Biol. 18, 544–550.
Baker, J.L., Celik, E., DeLisa, M.P., 2013. Expanding the glycoengineering toolbox: the rise of bacterial N-linked protein glycosylation. Trends Biotechnol. 31, 313–323.
Castillo-Hair, S.M., Sexton, J.T., Landry, B.P., Olson, E.J., Igoshin, O.A., Tabor, J.J., 2016. FlowCal: a user-friendly, open source software tool for automatically converting flow cytometry data from arbitrary to calibrated units. ACS Synth. Biol. 5, 774–780.
Celik, E., Fisher, A.C., Guarino, C., Mansell, T.J., DeLisa, M.P., 2010. A filamentous phage display system for N-linked glycoproteins. Protein Sci. 19, 2006–2013.
Dalziel, M., Crispin, M., Scanlan, C.N., Zitzmann, N., Dwek, R.A., 2014. Emerging principles for the therapeutic exploitation of glycosylation. Science 343, 1235681.
Durr, C., Nothaft, H., Lizak, C., Glockshuber, R., Aebi, M., 2010. The Escherichia coli glycophage display system. Glycobiology 20, 1366–1372.
Feldman, M.F., Wacker, M., Hernandez, M., Hitchen, P.G., Marolda, C.L., Kowarik, M., Morris, H.R., Dell, A., Valvano, M.A., Aebi, M., 2005. Engineering N-linked protein glycosylation with diverse O antigen lipopolysaccharide structures in Escherichia coli. Proc. Natl. Acad. Sci. USA 102, 3016–3021.
Fisher, A.C., Haitjema, C.H., Guarino, C., Celik, E., Endicott, C.E., Reading, C.A., Merritt, J.H., Ptak, A.C., Zhang, S., DeLisa, M.P., 2011. Production of secretory and extracellular N-linked glycoproteins in Escherichia coli. Appl. Environ. Microbiol. 77, 871–881.
Gao, N., 2005. Fluorophore-assisted carbohydrate electrophoresis: a sensitive and accurate method for the direct analysis of dolichol pyrophosphate-linked oligosaccharides in cell cultures and tissues. Methods 35, 323–327.
Gao, N., Lehrman, M.A., 2006. Non-radioactive analysis of lipid-linked oligosaccharide compositions by fluorophore-assisted carbohydrate electrophoresis. Methods Enzymol. 415, 3–20.
Gottesman, S., Trisler, P., Torres-Cabassa, A., 1985. Regulation of capsular polysaccharide synthesis in Escherichia coli K-12: characterization of three regulatory genes. J. Bacteriol. 162, 1111–1119.
Hamilton, B.S., Wilson, J.D., Shumakovich, M.A., Fisher, A.C., Brooks, J.C., Pontes, A., Naran, R., Heiss, C., Gao, C., Kardish, R., Heimburg-Molinaro, J., Azadi, P., Cummings, R.D., Merritt, J.H., DeLisa, M.P., 2017. A library of chemically defined human N-glycans synthesized from microbial oligosaccharide precursors. Sci. Rep. 7, 15907.
Hamilton, S.R., Bobrowicz, P., Bobrowicz, B., Davidson, R.C., Li, H., Mitchell, T., Nett, J.H., Rausch, S., Stadheim, T.A., Wischnewski, H., Wildt, S., Gerngross, T.U., 2003. Production of complex human glycoproteins in yeast. Science 301, 1244–1246.
Helenius, A., Aebi, M., 2001. Intracellular functions of N-linked glycans. Science 291, 2364–2369.
Ihssen, J., Kowarik, M., Dilettoso, S., Tanner, C., Wacker, M., Thony-Meyer, L., 2010. Production of glycoprotein vaccines in Escherichia coli. Microb. Cell Fact. 9, 61.
Ilg, K., Yavuz, E., Maffioli, C., Priem, B., Aebi, M., 2010. Glycomimicry: display of the GM3 sugar epitope on Escherichia coli and Salmonella enterica sv Typhimurium. Glycobiology 20, 1289–1297.
Kampf, M.M., Braun, M., Sirena, D., Ihssen, J., Thony-Meyer, L., Ren, Q., 2015. In vivo production of a novel glycoconjugate vaccine against Shigella flexneri 2a in recombinant Escherichia coli: identification of stimulating factors for in vivo glycosylation. Microb. Cell Fact. 14, 12.
Karlsson, A.J., Lim, H.K., Xu, H., Rocco, M.A., Bratkowski, M.A., Ke, A., DeLisa, M.P., 2012. Engineering antibody fitness and function using membrane-anchored display of correctly folded proteins. J. Mol. Biol. 416, 94–107.
Kelly, J.R., Rubin, A.J., Davis, J.H., Ajo-Franklin, C.M., Cumbers, J., Czar, M.J., de Mora, K., Glieberman, A.L., Monie, D.D., Endy, D., 2009. Measuring the activity of BioBrick promoters using an in vivo reference standard. J. Biol. Eng. 3, 4.
Keys, T.G., Aebi, M., 2017. Engineering protein glycosylation in prokaryotes. Curr. Opin.

Syst. Biol. 5, 23–31.
Lucks, J.B., Qi, L., Mutalik, V.K., Wang, D., Arkin, A.P., 2011. Versatile RNA-sensing transcriptional regulators for engineering genetic networks. Proc. Natl. Acad. Sci. USA 108, 8617–8622.
Merritt, J.H., Ollis, A.A., Fisher, A.C., DeLisa, M.P., 2013. Glycans-by-design: engineering bacteria for the biosynthesis of complex glycans and glycoconjugates. Biotechnol. Bioeng. 110, 1550–1564.
Meuris, L., Santens, F., Elson, G., Festjens, N., Boone, M., Dos Santos, A., Devos, S., Rousseau, F., Plets, E., Houthuys, E., Malinge, P., Magistrelli, G., Cons, L., Chatel, L., Devreese, B., Callewaert, N., 2014. GlycoDelete engineering of mammalian cells simplifies N-glycosylation of recombinant proteins. Nat. Biotechnol. 32, 485–489.
Mills, D.C., Jervis, A.J., Abouelhadid, S., Yates, L.E., Cuccui, J., Linton, D., Wren, B.W., 2016. Functional analysis of N-linking oligosaccharyl transferase enzymes encoded by deep-sea vent proteobacteria. Glycobiology 26 (4), 398–409.
Mimura, Y., Katoh, T., Saldova, R., O'Flaherty, R., Izumi, T., Mimura-Kimura, Y., Utsunomiya, T., Mizukami, Y., Yamamoto, K., Matsumoto, T., Rudd, P.M., 2018. Glycosylation engineering of therapeutic IgG antibodies: challenges for the safety, functionality and efficacy. Protein Cell 9 (1), 47–62.
Na, D., Yoo, S.M., Chung, H., Park, H., Park, J.H., Lee, S.Y., 2013. Metabolic engineering of Escherichia coli using synthetic small regulatory RNAs. Nat. Biotechnol. 31, 170–174.
Ollis, A.A., Chai, Y., Natarajan, A., Perregaux, E., Jaroentomeechai, T., Guarino, C., Smith, J., Zhang, S., DeLisa, M.P., 2015. Substitute sweeteners: diverse bacterial oligosaccharyltransferases with unique N-glycosylation site preferences. Sci. Rep. 5, 15237.
Ollis, A.A., Zhang, S., Fisher, A.C., DeLisa, M.P., 2014. Engineered oligosaccharyl-transferases with greatly relaxed acceptor-site specificity. Nat. Chem. Biol. 10, 816–822.
Rich, J.R., Withers, S.G., 2009. Emerging methods for the production of homogeneous human glycoproteins. Nat. Chem. Biol. 5, 206–215.
Rudd, P.M., Dwek, R.A., 1997. Glycosylation: heterogeneity and the 3D structure of proteins. Crit. Rev. Biochem. Mol. Biol. 32, 1–100.
Sethuraman, N., Stadheim, T.A., 2006. Challenges in therapeutic glycoprotein production. Curr. Opin. Biotechnol. 17, 341–346.
Shanks, R.M., Caiazza, N.C., Hinsa, S.M., Toutain, C.M., O'Toole, G.A., 2006. Saccharomyces cerevisiae-based molecular tool kit for manipulation of genes from gram-negative bacteria. Appl. Environ. Microbiol. 72, 5027–5036.
Song, T., Aldredge, D., Lebrilla, C.B., 2015. A method for in-depth structural annotation of human serum glycans that yields biological variations. Anal. Chem. 87, 7754–7762.
Strohalm, M., Hassman, M., Kosata, B., Kodicek, M., 2008. mMass data miner: an open source alternative for mass spectrometric data analysis. Rapid Commun. Mass Spectrom. 22, 905–908.
Terra, V.S., Mills, D.C., Yates, L.E., Abouelhadid, S., Cuccui, J., Wren, B.W., 2012. Recent developments in bacterial protein glycan coupling technology and glycoconjugate vaccine design. J. Med. Microbiol. 61, 919–926.
Valderrama-Rincon, J.D., Fisher, A.C., Merritt, J.H., Fan, Y.Y., Reading, C.A., Chhiba, K., Heiss, C., Azadi, P., Aebi, M., DeLisa, M.P., 2012. An engineered eukaryotic protein glycosylation pathway in Escherichia coli. Nat. Chem. Biol. 8, 434–436.
Wacker, M., Linton, D., Hitchen, P.G., Nita-Lazar, M., Haslam, S.M., North, S.J., Panico, M., Morris, H.R., Dell, A., Wren, B.W., Aebi, M., 2002. N-linked glycosylation in Campylobacter jejuni and its functional transfer into E. coli. Science 298, 1790–1793.
Wang, H.H., Isaacs, F.J., Carr, P.A., Sun, Z.Z., Xu, G., Forest, C.R., Church, G.M., 2009. Programming cells by multiplex genome engineering and accelerated evolution. Nature 460, 894–898.
Wormald, M.R., Dwek, R.A., 1999. Glycoproteins: glycan presentation and protein-fold stability. Structure 7, R155–R160.
Xu, C., Ng, D.T., 2015. Glycosylation-directed quality control of protein folding. Nat. Rev. Mol. Cell Biol. 16, 742–752.
Yang, Z., Wang, S., Halim, A., Schulz, M.A., Frodin, M., Rahman, S.H., Vester-Christensen, M.B., Behrens, C., Kristensen, C., Vakhrushev, S.Y., Bennett, E.P., Wandall, H.H., Clausen, H., 2015. Engineered CHO cells for production of diverse, homogeneous glycoproteins. Nat. Biotechnol. 33, 842–844.
Zhang, P., Woen, S., Wang, T., Liau, B., Zhao, S., Chen, C., Yang, Y., Song, Z., Wormald, M.R., Yu, C., Rudd, P.M., 2016. Challenges of glycosylation analysis and control: an integrated approach to producing optimal and consistent therapeutic drugs. Drug Discov. Today 21 (5), 740–765.